Article

Not peer-reviewed version

Research on the Preparation of Supercapacitor Separators with High Wettability and Excellent Temperature Adaptability through In Situ Deposition of Nano-Barium Sulfate on Regenerated Cellulose

Hui Li , Jiehua Li , Chuanshan Zhao * , Fenfen Zhao *

Posted Date: 21 February 2025

doi: 10.20944/preprints202502.1660.v1

Keywords: separators; lyocell fibers; fibrillation; nano-barium sulfate; physical properties; ionic properties; charge–discharge performance; temperature adaptability

 doi:10.20944/preprints202502.1660.v1

Article

Research on the Preparation of Supercapacitor Separators with High Wettability and Excellent Temperature Adaptability through In Situ Deposition of Nano-Barium Sulfate on Regenerated Cellulose

Hui Li [1], Jiehua Li [1], Chuanshan Zhao [1]* and Fenfen Zhao [2]*

[1] State Key Laboratory of Green Papermaking and Resource RecyclingQilu University of Technology, Shandong Academy of Sciences, Jinan 250353

[2] Shandong Shenghan Finance and Trade Vocational College, Jinan 250316

* Correspondence: ppzcs78@163.com (C.Z.); 503029640@qq.com (F.Z.)

Abstract: With portable electronics and new-energy vehicles booming, the demand for high-performance energy storage devices has skyrocketed. Supercapacitor separators are thus vital. Traditional ones such as polyolefins and non-woven fabrics have limitations, while cellulose and its derivatives, with low cost, good hydrophilicity, and strong chemical stability, are potential alternatives. This study used regenerated cellulose Lyocell fibers. Through fiber treatment, refining, and in situ deposition, a composite regenerated cellulose separator (NFRC-Ba) with nano-barium sulfate was made. Its physical, ionic, and charge–discharge properties were tested. The results show that NFRC-Ba excels in terms of mechanical strength, porosity, hydrophilicity, and thermal stability. Compared with the commercial NKK30AC-100 separator, it has better ionic conductivity, better ion-transport ability, a higher specific capacitance, better capacitance retention, and good cycle durability. It also performs stably from -40°C to 100°C. With a simple and low-cost preparation process, NFRC-Ba could be a commercial separator for advanced supercapacitors.

Keywords: separators; lyocell fibers; fibrillation; nano-barium sulfate; physical properties; ionic properties; charge–discharge performance; temperature adaptability

1. Introduction

Currently, the portable electronic device and new - energy vehicle sectors are experiencing rapid expansion and are developing with strong impetus. Energy storage devices have become one of the most crucial materials in these fields. It is anticipated that these devices will possess the characteristics of high charge - storing capacity and high power density[1-3]. Among a wide array of energy storage devices, supercapacitors are regarded as highly promising. Commonly seen examples include graphene helium-ion batteries, fuel cells, solid-state electrolytic capacitors, etc., [. Given its intrinsic functional attributes, the separator assumes a position of paramount significance within the framework of supercapacitors. Functionally, it serves a dual-purpose role: acting as a physical safeguard barrier positioned between the two electrodes while concurrently creating a conductive pathway that facilitates the effective transportation of ions [9-14]. Consequently, the structural characteristics and inherent properties of the separator play pivotal and decisive roles in determining the overall performances of supercapacitors (SCs). In the pursuit of high-performance supercapacitors, an ideal separator is expected to exhibit a combination of remarkable features. These include high mechanical strength to ensure structural integrity during operation, high porosity to facilitate efficient ion transport, good hydrophilicity to enhance electrolyte wettability, excellent

 doi:10.20944/preprints202502.1660.v1

thermal stability to maintain its functionality under varying temperature conditions, and stable chemical properties to resist degradation and ensure long-term reliability [15-18].

Nevertheless, attributable to the exacting demands placed on them, separators endowed with all advanced properties have, to a large extent, remained inadequately explored. Up to the present, two principal categories of separators have found the most extensive application in commercial supercapacitors: polyolefins and non-woven fabrics [19-21]. Polyolefin - based materials, like the polypropylene (PP) separators, possess a certain degree of durability. Nevertheless, given their relatively low glass - transition and melting temperatures, they undergo shrinkage under high - temperature conditions. Additionally, their subpar porosity and hydrophilicity act as barriers to ion transportation. In contrast, non - woven supercapacitor separators, for example, non - woven polypropylene variants, feature favorable porosity and hydrophilicity. However, the melt-blown manufacturing process gives them low mechanical strength and reliability, reducing safety and stability. To overcome these formidable bottlenecks, extensive research efforts have been dedicated to exploring advanced manufacturing methodologies and refinement techniques for separators. In the contemporary research landscape, diverse coated and cross-linked polyolefin [21] separators have emerged as focal points of investigation [22-24]. Nevertheless, by virtue of the inborn constraints intrinsic to polyolefin-based separators, the high-temperature performance of composite separators remains sub-optimal. Glass fiber separators, renowned for their elevated ionic conductivity, superior electrolyte uptake capacity, and commendable thermal stability, are often employed as separators. However, their prohibitively high cost and overly substantial thickness pose formidable impediments to their large-scale industrial implementation [25-27]. Consequently, a body of research has delved into methodologies including electrospinning [28-30] and bio-exfoliation. The overarching objective is to engender novel morphological configurations of separators, thereby circumventing the existing limitations inherent within this domain [31-34]. Regrettably, these preparation processes are complex, costly, and hard to scale up. Thus, developing advanced separators with low cost, environmental friendliness, and excellent overall performance remains a formidable challenge. This challenge, deeply rooted in materials science, manufacturing, and chemical technology, requires profound insights, innovation, and interdisciplinary methods to overcome technological bottlenecks and advance separator development.

Cellulose, the most copiously abundant biodegradable natural macromolecular material on Earth, is considered one of the viable candidates for separator materials. This is ascribable to its inexpensive cost, favorable hydrophilic characteristics, and robust chemical stability. The unique combination of these attributes positions cellulose at the forefront of research for separator applications, having the potential to address some of the key limitations in existing separator technologies [35, 36]. Several cellulose derivatives including cellulose acetate, methylcellulose, and microcrystalline cellulose have been made into battery separators through either electrospinning or phase - inversion methods. [37-39]. The regenerated cellulose separator, with strong hydrogen bonds and significant van der Waals forces, exhibits outstanding mechanical strength and thermal stability. This effectively addresses the mechanical strength limitations inherent in cellulose-based separators. Extensive research on regenerated cellulose separators has underscored their substantial potential for applications in separators, thereby providing significant impetus to the exploration of novel high-performance cellulose separators. Lyocell fiber, a type of regenerated cellulose fiber, is prone to fibrillation when subjected to shear forces, such as those experienced in the wet state or during mechanical abrasion caused by external forces [40]. This phenomenon can be ascribed to the high axial orientation degree of Lyocell fibers, accompanied by a relatively feeble transverse bonding force between microfibrils. When in the wet state, the occurrence of fiber swelling further exacerbates the weakening of this bonding force. As a consequence, the cortical fibers tend to shed, and the remaining cortical fibers experience longitudinal fissuring, ultimately leading to the formation of non-homogeneous fibrillated fibers [41]. The fibrillar structures formed after fibrillation can intricately intermesh, significantly enhancing the separator material's overall mechanical strength and enabling better structural stability in battery-like applications. This material features tunable pore sizes,

 doi:10.20944/preprints202502.1660.v1

suitable porosity, excellent wettability, and high thermal stability. Presently, it has emerged as a novel candidate for supercapacitor separator research, with great potential to improve energy storage performance [42, 43].

Nanocellulose, derived from natural plant resources such as wood and cotton, boasts the characteristics of renewability and biodegradability. In contrast to conventional petroleum-based separator materials, it is more eco-friendly and aligns well with the imperatives of sustainable development [36, 44, 45]. Nanocellulose inherently has high strength and high modulus. Once integrated into the separator, it can interact with the separator's matrix material via hydrogen bonds, van der Waals forces, and so on, creating a three - dimensional network structure. This interaction boosts the separator's overall mechanical properties, like tensile strength and puncture resistance. As a result, the separator can more effectively preserve its structural integrity throughout the battery's charge - discharge cycles. Meanwhile, nanocellulose can enhance the thermal stability of the material and regulate its pore structure [46-50].

Barium sulfate, with its excellent high-temperature resistance and fireproof performance, can stabilize the separator in high-temperature environments, averting the shrinkage or melting of polyolefin-based separators at high temperatures that could lead to battery short-circuits, thereby significantly enhancing battery safety. Additionally, it can improve electrolyte affinity and promote lithium-ion transport, rendering it applicable as a reinforcing additive in separator research [51-54].

In this study, regenerated cellulose Lyocell fibers served as the fundamental raw materials. Through a series of meticulous procedures involving fiber treatment and refining, nanofibrillated fibers with precisely controlled diameters ranging from 1 to 2 μm were successfully fabricated. Subsequently, a unique in situ deposition technique was employed to generate nano-barium sulfate particles within the nanocellulose matrix. These newly formed nano-particles were then homogeneously blended with the nanofibrillated fibers, and a composite regenerated cellulose separator was crafted using the papermaking process. This newly developed separator showcases remarkable physical and chemical properties. It features a highly uniform porous NFRC-Ba architecture, which not only contributes to its enhanced electrolyte permeability but also plays a crucial role in maintaining structural integrity. Moreover, it demonstrates superior mechanical strength, ensuring its durability under various operating conditions. The separator also exhibits excellent electrolyte wettability, facilitating efficient ion transfer, and outstanding thermal stability, enabling reliable performance over a wide temperature range. When benchmarked against a commercial NFRC-Bai non-woven separator (NKK30AC-100), this composite separator outperforms others in terms of ion transport characteristics. It achieves higher ion conductivity, leading to more rapid charge–discharge processes. Additionally, it possesses a higher capacitance value and remarkable capacitance retention ability, which are essential for long-term and stable energy storage applications. Moreover, the electrochemical performance of the composite regenerated cellulose separator was comprehensively evaluated in environments of both high and low temperatures. The results reveal an impressively wide operating temperature range, spanning from a cold -40°C to a relatively high 100°C. This broad temperature adaptability significantly expands the separator’s potential applications in extreme-condition scenarios. Most notably, the preparation process of this composite regenerated cellulose separator is characterized by its simplicity and cost-effectiveness. With the availability of special papermaking equipment, it holds great promise for large-scale industrial production. In conclusion, the composite regenerated cellulose (NFRC-Ba) separator, boasting such outstanding performance attributes, is highly anticipated to emerge as a leading commercial NFRC-Ba material for advanced NFRC-Ba supercapacitors and other high-performance, high-safety capacitor separators in the market.

 doi:10.20944/preprints202502.1660.v1

2. Materials and Methods

2.1. Materials and Reagents

Lyocell fibers (CLY), supplied by Shandong Boao New Material Co., Ltd. (Linqing, China), had an average length of 4 mm and a diameter of 1.33 denier. Nanocellulose (NFC), with a length ranging from 0.5 to 1 μm and a diameter of 50-100 nm, was NFRC-Ba purchased from Shandong Shengquan Group (Jinan, China). Sodium sulfate (analytical reagent, AR) and barium chloride (analytical reagent, AR) were procured from Sinopharm Chemical Reagent Co., Ltd. (Shanghai, China).

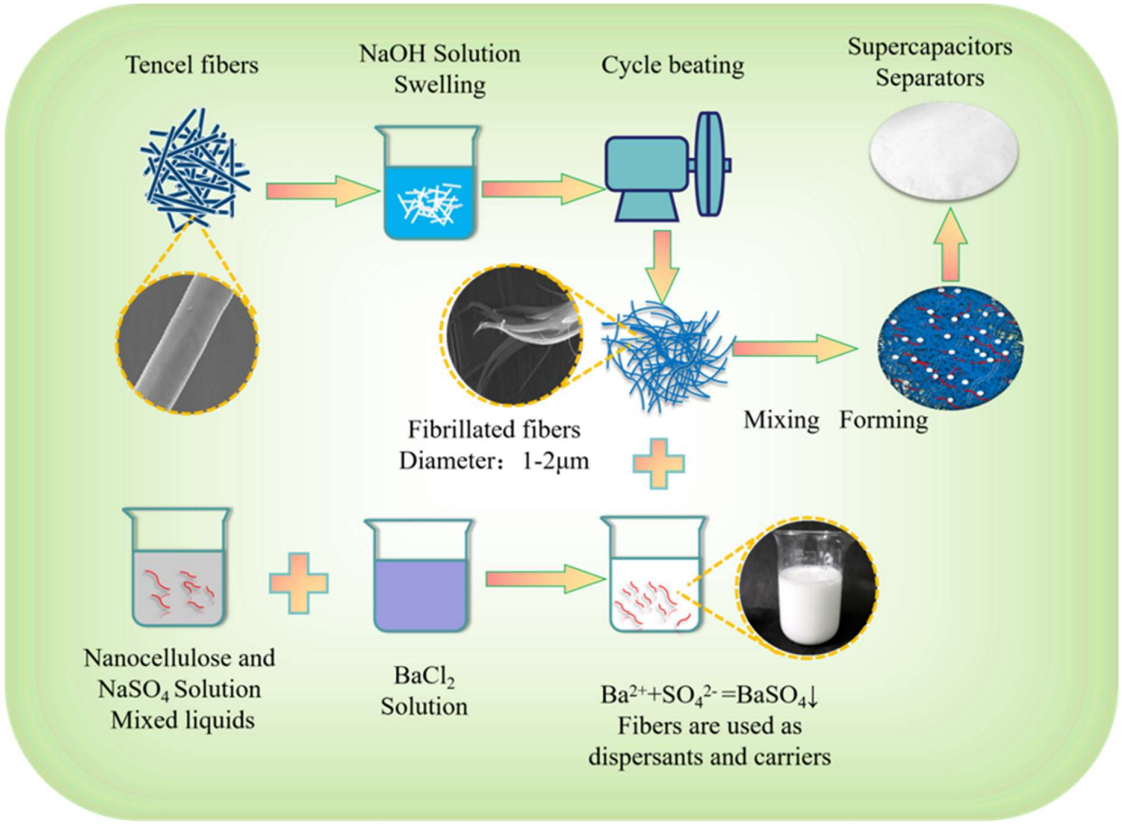

Figure 1. The preparation process of the composite regenerated cellulose separator paper.

2.2. Preparation of Composite Regenerated Cellulose Separator

1. Immerse Lyocell fibers (CLY) in a 1 wt% sodium hydroxide solution for 2 hours to enable the fibers to fully absorb the solution and swell, thereby weakening the hydrogen bond binding NFRC-Ba between the fibers. Subsequently, prepare the treated CLY into a fiber slurry with a concentration of 10 wt% and feed it into a refiner for a meticulous refining treatment of 80,000 revolutions. Through this operation, the fibers can be fully fibrillated, ultimately separating into nanofibrillated Lyocell fibers (MCLY) with diameters ranging from 1 to 2 μm.
2. Carefully prepare a 1 mol/L sodium sulfate solution and a 1 mol/L barium chloride solution. Add the sodium sulfate solution to the 3 wt% NFC mixture at a ratio of 5:5. Then, use an ultrasonic disperser to ensure that the NFC is fully dispersed in the liquid. After that, mix the two solutions uniformly according to a molar ratio of sulfate ions (SO42-) to barium ions (Ba2+) of 1:1, so as to carry out in situ nano-barium sulfate precipitation within the NFC system and successfully prepare an NFC-BA mixture.
3. Thoroughly mix MCLY and NFC-Ba at a precise ratio of 7:3 and then prepare a homogeneous liquid with a fiber concentration of 0.3 wt%. Utilize a special papermaking machine to produce a composite regenerated cellulose separator paper (NFNFRC-Ba) with a basis weight of 13 g/m². Meanwhile, use only MCLY as the raw material to prepare a cellulose separator paper (FNFRC-

 doi:10.20944/preprints202502.1660.v1

Ba) with the same basis weight of 13 g/m² as the control sample. The detailed preparation process of the composite regenerated cellulose separator paper (NFNFRC-Ba) is shown in Figure 1.

3. Results

3.1. Physical Properties of the NFRC-Ba

The mechanical strength of the separator is a pivotal parameter that exerts a profound influence on the safety of supercapacitors. An optimal separator is expected to possess adequate mechanical robustness to withstand potential damage during the assembly procedures and normal-use collisions [55]. Initially, a comparative analysis was conducted on the stress–strain curves of the NFRC-Ba and the FRC separator, as presented in **Figure 2a**. The FRC exhibited an overall breaking strength of merely 20.46 MPa. In stark contrast, the NFRC-Ba achieved an overall breaking strength of 47.25 MPa, marking a substantial 130.93% increase relative to the FRC separator. Furthermore, a tensile experiment utilizing a 200 g weight provided empirical evidence that the NFRC-Ba separator manifested commendable dimensional stability and remarkable mechanical strength.

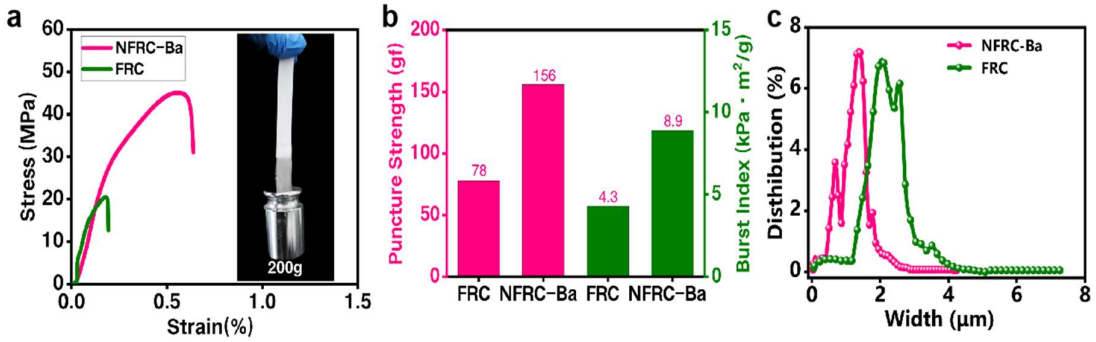

Figure 2. Physical strength and pore size distribution of NFRC-Ba and FRC separators: (a) stress–strain curve of NFRC-Ba/FRC separators; (b) bursting strength and puncture strength of NFRC-Ba/FRC separators; (c) pore size distribution of NFRC-Ba/FRC separators.

Concurrently, the NFRC-Ba separator demonstrated pre-eminent puncture strength and bursting strength. As clearly illustrated in **Figure 2b**, the FRC separator had an overall puncture strength of 78 gf and a bursting strength of 4.3 KPa·m²/g. In comparison, the NFRC-Ba boasted a puncture strength of 156 gf and a bursting strength of 8.9 KPa·m²/g, which were 2-fold and 2.1-fold higher than those of the FRC separator, respectively. This superior mechanical performance was instrumental in preserving the structural integrity of the separator during unforeseen collisions and averting rupture, thereby contributing significantly to the enhancement of battery safety [56, 57].

The underlying mechanism for this disparity in mechanical strength is as follows: CLY fibers, being regenerated cellulose fibers, feature smooth surfaces with a limited number of exposed hydroxyl groups. This characteristic leads to feeble hydrogen-bonding interactions between adjacent fibers. As a consequence, the FRC separator fabricated solely from MCLY fibers exhibits suboptimal mechanical strength. In the case of NFRC-Ba, the incorporation of NFC as a fiber-reinforcing additive has yielded remarkable results. It is well established within the realm of nanocellulose research that NFC serves as an effective inter-fiber adhesive. By increasing the density of hydroxyl groups, NFC strengthens the hydrogen-bonding forces between fibers, thereby enhancing the overall mechanical performance of the separator.

The separator's uniform pore size and elevated porosity establish a secure and stable conduit for ion transport. This not only enables the retention of a substantial quantity of electrolyte but also bolsters the ion-shuttling effect, thereby enhancing the cycling performance and rate capability of supercapacitors. **Figure 2c** illustrates the pore-size distribution profiles of the NFRC-Ba and FRC separators. Evidently, the NFRC-Ba separator exhibits a relatively narrow pore-size distribution,

 doi:10.20944/preprints202502.1660.v1

predominantly concentrated within the range of 0.6 μm to 2 μm. The corresponding distribution curve presents a solitary, well-defined peak, which is proximate to the median value of the pore-size distribution. Conversely, the FRC separator displays a broader distribution, extending from 1.3 μm to 3.5 μm. Its distribution curve features two peaks, signifying a comparatively poor uniformity in pore-size distribution. The porosity of the fabricated FRC membrane is approximately 56.7%, whereas that of the NFRC-Ba membrane is around 81.3%. This value far exceeds the porosities of the commercial NKK30AC-100 separator (53.4%) and the Celgard 2500 separator (38%). The NFRC-Ba separator's manifestation of a uniform pore size and superior porosity can be ascribed to the presence of finer fibrillated fibers and the incorporation of nano-$BaSO_4$. These factors augment the specific surface area within the structure. Moreover, the introduction of nanocellulose enriches the hydrophilic groups ($-$ OH), thereby enhancing hydrophilicity. In conclusion, the NFRC-Ba separator's uniform pore size and high porosity underscore its substantial potential for applications in advanced supercapacitors and batteries.

The electrolyte wettability of the separator is a pivotal parameter that exerts a profound influence on both the electrochemical performance of supercapacitors and their assembly processes [58]. The wetting characteristics of diverse separators were meticulously evaluated via contact angle (CA) measurements. As illustrated in **Figure 3a**, the contact angle of a water droplet on the NFRC-Ba membrane was initially measured to be 9.2°. Intriguingly, this value reduced to zero within a mere 5-second interval, demonstrating the exceptional hydrophilicity of the NFRC-Ba membrane. Owing to its pronounced affinity with the electrolyte and its high-porosity attributes, the NFRC-Ba separator showcased pre-eminent electrolyte wettability. This property effectively expedited the infiltration of the electrolyte, thereby augmenting the ionic transport rate within the separator [59]. Conversely, the NKK30AC-100 separator exhibited a contact angle of 41.5°, while the Celgard 2500 membrane registered a contact angle of 53.7°, signifying their relatively inferior hydrophilicity.

The morphologies of the synthesized FRC and NFRC-Ba membranes were examined via scanning electron microscopy (SEM) (**Figure 3d-1, 3d-2**). The NFRC-Ba membrane has a more compact and uniform surface than the FRC. Nanocellulose fibrils (NFCs) connect and reinforce, filling spaces between fibrillated fibers, with substantial nano-barium sulfate samples deposited. The magnified SEM image (**Figure 3d-3**) shows a uniformly distributed pore structure with a narrow size range. Pores form a 3D tortuous network via multi-layer interlacing, increasing porosity and enabling uniform ion migration between electrodes. Energy-dispersive spectroscopy (EDS) validates the homogeneous dispersion of nano-$BaSO_4$ in the NFRC-Ba membrane through S and Ba element distribution. Precisely controlling nanocellulose and nano-$BaSO_4$ amounts can optimize pore distribution and size. Isolated pores may shorten ion-diffusion paths, reducing ion–ion collisions and enhancing supercapacitor (SC) performance [60, 61]. Interestingly, in the NFRC-Ba membrane, nanocellulose fills inter-fiber gaps and adheres to fiber surfaces, likely due to strong hydrogen-bonding-mediated self-aggregation. This boosts both mechanical strength and flexibility. This unique structure benefits supercapacitors by strengthening the membrane, increasing porosity, and facilitating electrolyte adsorption and ion transport.

 doi:10.20944/preprints202502.1660.v1

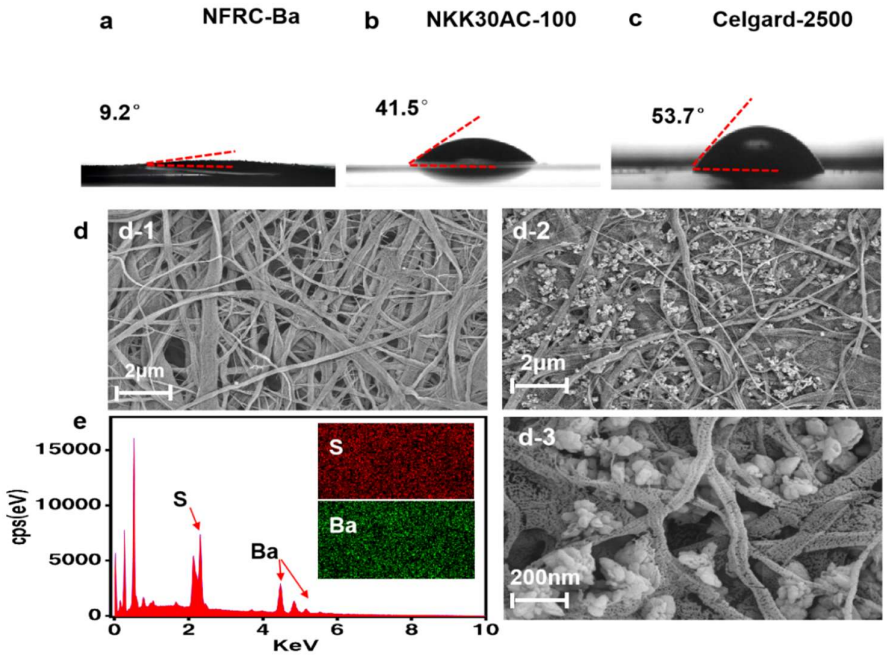

Figure 3. The electrolyte wettability tests of different separators: (a) NFRC-Ba separator; (b) NKK30AC-100 separator; (c) Celgard 2500 separator. SEM and EDS images of the surfaces of the NFRC-Ba and FRC separators: (d-1) SEM of FRC separators at low magnification; (d-2) SEM of NFRC-Ba separators at low magnification; (d-3) SEM of NFRC-Ba separators at higher magnification; (e) EDS distribution of S and Ba of NFRC-Ba separators.

In the realm of supercapacitor safety, the thermal stability of the separator assumes paramount significance, particularly in high-power and high-energy applications. During the charge–discharge cycles of supercapacitors, the liberated heat can inflict damage upon the separator, thereby precipitating potential short-circuits or even explosions [62]. **Figure 4a** illustrates that the NFRC-Ba separator undergoes negligible shrinkage within the temperature spectrum from ambient to 180 °C, registering a shrinkage rate of less than 3%. Even subsequent to multiple reiterative heating treatments, it effectively sustains its shape and dimensions. In stark contrast, the NKK30AC-100 separator can uphold thermal stability up to 140 °C; however, it begins to wrinkle at 150 °C and melts at 180 °C (**Figure 4b**). The Celgard 2500 separator initiates thermal shrinkage at 120 °C and melts at 150 °C (**Figure 4c**). These outcomes show that, due to the pre-eminence of its raw materials and manufacturing techniques, the NFRC-Ba separator boasts exceptional thermal stability. This attribute is indispensable for mitigating the safety perils associated with supercapacitors and other batteries operating at elevated temperatures.

Collectively, the aforesaid results insinuate that the NFRC-Ba separator, distinguished by its superior mechanical properties, uniform pore size, excellent porosity, high-efficiency electrolyte wettability, and remarkable thermal stability, holds promise for emerging as a propitious candidate material for commercial supercapacitor separators.

 doi:10.20944/preprints202502.1660.v1

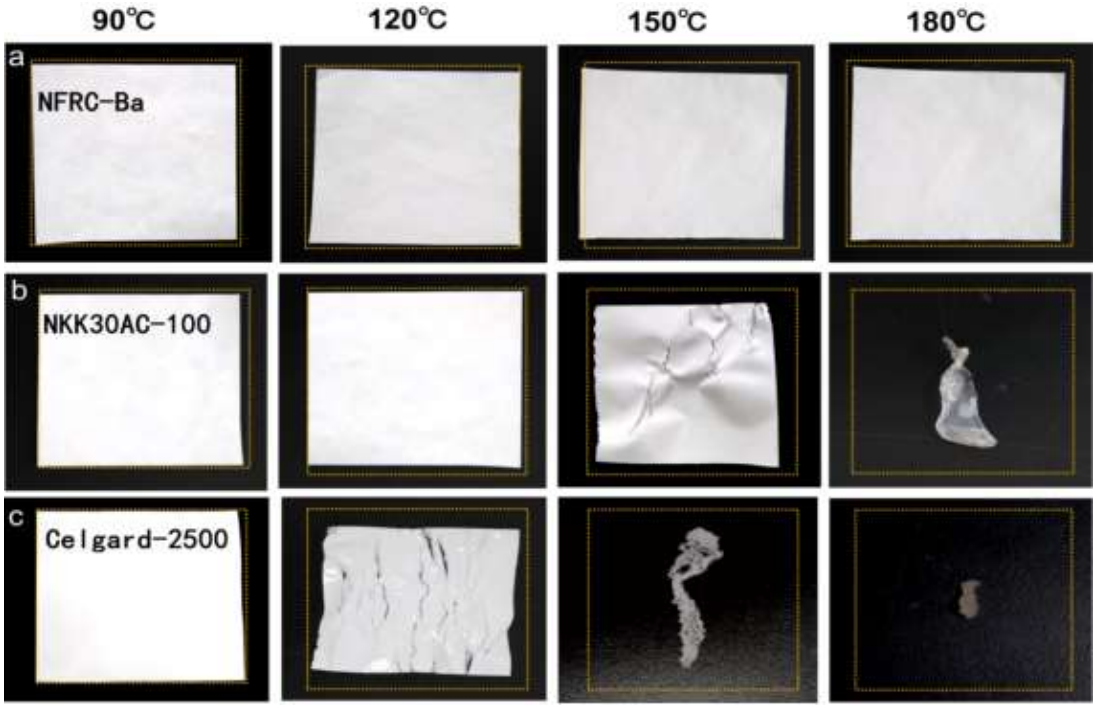

Figure 4. An illustration of the thermal shrinkages of the separators at different temperatures: (a) NFRC-Ba separator; (b) NKK30AC-100 separator; (c) Celgard 2500 separator.

3.2. Ionic Property of the NFRC-Ba Separator

The ionic conductivities of the NFRC-Ba separator, Celgard 2500 separator, and NKK30AC-100 separator were determined through electrochemical impedance spectroscopy (EIS) within a sandwich-structured configuration, namely stainless-steel (SS)/separator/stainless-steel. As presented in **Figure 5a**, the EIS data elucidate that the ionic conductivity of the NFRC-Ba separator is 9.25 mS/cm. This value is closely akin to that of the commercial NKK30AC-100 separator, registered at 8.72 mS/cm, and substantially surpasses that of the Celgard 2500 separator, measured at 1.68 mS/cm. It is widely recognized within the scientific community that the ionic conductivity of a separator is, to a significant degree, governed by its wettability with respect to the electrolyte, absorption capacity, and porosity [63]. A higher ionic conductivity serves to expedite the swift transport of ions across the separator, thereby playing a pivotal role in the electrochemical performance of the associated system.

 doi:10.20944/preprints202502.1660.v1

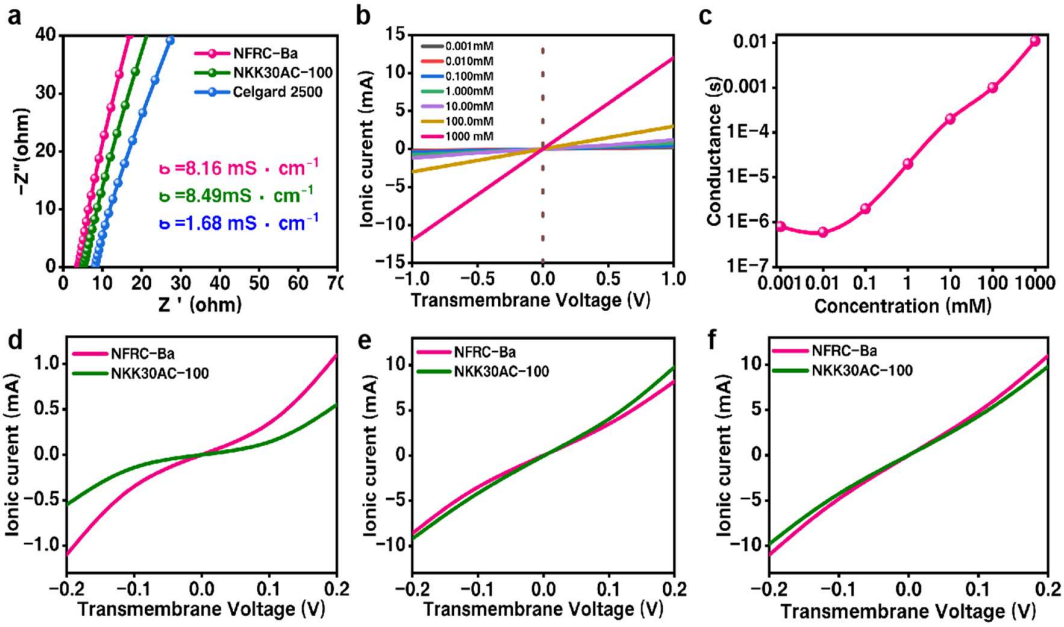

Figure 5. Ion Transport in Various Separators：(a) Electrochemical impedance spectroscopy (EIS) of the NFRC - Ba, NKK30AC - 100, and Celgard 2500 separators was utilized to calculate ionic conductivity；(b) The ionic current - voltage (I - V) behaviors of the NFRC - Ba separator were measured in KCl electrolytes with varying concentrations；(c) The transmembrane ion conductance of the separator was investigated as a function of electrolyte concentration. The I - V curves of the NFRC - Ba and NKK30AC - 100 separators were obtained in commercial aqueous electrolytes: (d) 1.0 mol/L Na_2SO_4；(e) 1.0 mol/L H_2SO_4, and (f) 6.0 mol/L KOH.

Numerous studies have demonstrated that the diffusion of ions through nanoporous materials can be significantly influenced by a local electric field generated by surface charges [64]. In light of this, the ion - transport behavior of the NFRC - Ba separator was meticulously investigated using a well - established ionic current measurement technique. The aqueous KCl solution was selected as the electrolyte due to the comparable diffusion coefficients of K^+ and Cl^- ions because of the similar values of diffusion coefficient between the $K^+$and Cl^- ions [65].As vividly illustrated in **Figure 5b**, the ionic current - voltage (I - V) curves at various concentrations exhibit distinct linear ohmic characteristics, clearly indicating the presence of trans - separator ionic conductance. It has been determined that the ionic conductance of the bulk electrolyte is directly proportional to the concentration of the KCl electrolyte (**Figure 5c**). To be more specific, within the high - concentration regime, the ionic conductance adheres to the bulk rule, demonstrating a linear relationship. However, as the concentration gradually decreases, at 0.1 mM, the measured ionic conductance begins to deviate from the bulk value. More precisely, when the concentration of the electrolyte exceeds 0.1 mM, the surface charges have minimal control over the trans - separator ionic transport. This effectively confirms that the impact of surface charges on the practical application of the NFRC - Ba separator is negligible.

When the Debye - Hückel approximation is applied, one can notice that at high concentrations, the Debye screening length of the channels shrinks, getting closer to electrical neutrality. In contrast, at low concentrations, the electrical potential generated by surface charges causes the Debye screening length to increase. Furthermore, a specially designed cell was built to examine the ion - transport capabilities of different separators in commercial aqueous electrolytes, namely 1.0 mol/L Na_2SO_4, 1.0 mol/L H_2SO_4, and 6.0 mol/L KOH. As depicted in Figures 5d and 5e, the current - voltage (I - V) curves demonstrate that the NFRC - Ba separator exhibits a significantly higher ionic current compared to the NKK - MPF30AC - 100 separator. Thanks to the large number of hydrophilic groups (-OH) and a greater number of ion - transport channels, the ion - transport and permeability of the

 doi:10.20944/preprints202502.1660.v1

NFRC - Ba separator in the 1.0 mol/L Na_2SO_4 electrolyte are 2.5 times higher than those of the commercial reference separators. In the 6.0 mol/L KOH electrolyte, the NFRC - Ba separator has a lower ionic current. This might be because the negative surface charge restricts the transport of OH^- ions.

3.3. Charge–Discharge Performance of the NFRC-Ba Separator

To assess the potential commercial feasibility of the NFRC - Ba separator, symmetric supercapacitors were assembled, using the NFRC - Ba separator and the commercial NKK30AC - 100 separator. The electrochemical characteristics of the manufactured supercapacitors were evaluated through cyclic voltammetry (CV), galvanostatic charge - discharge (GCD), and electrochemical impedance spectroscopy (EIS) measurements. Given that the electrodes and electrolytes were uniform in all devices, any differences in the performance of the batteries could be attributed to the unique features of the separators.

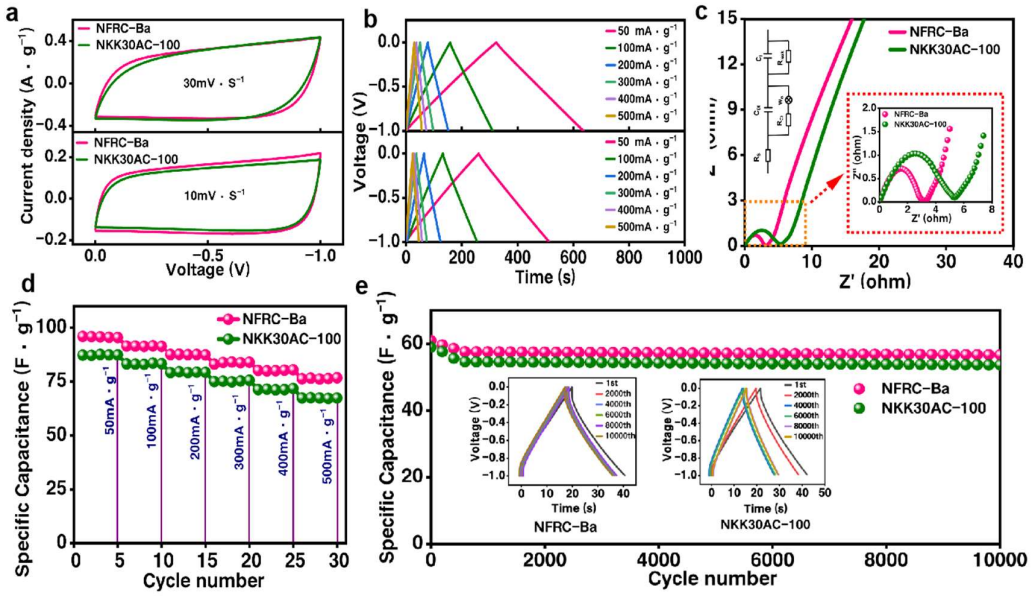

Figure 6. Comparison of Electrochemical Properties between the NFRC - Ba Separator and the Commercial NKK30AC - 100 Separator in a 1.0 mol/L Na_2SO_4 Electrolyte: (a) Cyclic voltammograms (CVs) of NFRC - Ba and NKK30AC - 100 at different scan rates (10, 30 mV /s); (b) Galvanostatic charge - discharge (GCD) curves of NFRC - Ba and NKK30AC - 100 at various current densities ranging from 50 to 500 mA /g; (c) Electrochemical impedance spectroscopy (EIS) curves of NFRC - Ba and NKK30AC - 100; (d) Specific capacitances of NFRC - Ba and NKK30AC - 100 at different current densities; (e) Long - term cycling performances of NFRC - Ba and NKK30AC - 100 under a current density of 1 A /g.

Figure 6a illustrates the cyclic voltammetry (CV) curves of the fabricated supercapacitors immersed in a 1.0 M sodium sulfate electrolyte, acquired at scan rates of 10 mV/s and 30 mV/s. With the increase in the scan rate, the NFRC-Ba separator demonstrates enhanced rate performance, as evidenced by its near-rectangular CV curve profile. In stark contrast, the CV curve of the NKK30AC-100 separator undergoes notable distortion, signifying its relatively poor rate performance, which can be attributed to the elevated equivalent series resistance (ESR) within the device. Conversely, the NFRC-Ba separator a quasi-rectangular CV curve, indicating a rapid current response upon voltage reversal, thereby suggesting the low ESR of the device. Moreover, the area encompassed by the CV curve of the NFRC-Ba separator is considerably larger than that of the NKK30AC-100 separator. This disparity in enclosed area is indicative of a higher specific capacitance for the NFRC-Ba separator. At

 doi:10.20944/preprints202502.1660.v1

a scan rate of 10 mV/s, the specific capacitance of the NFRC-Ba separator is approximately 32.45 F/g, surpassing that of the NKK30AC-100 separator, which measures at 26.72 F/g. When the scan rate is increased to 30 mV/s, the capacitance retention rate of the NFRC-Ba separator reaches 81.25%, markedly higher than the 72.98% capacitance retention rate of the NKK30AC-100 separator.

Galvanostatic charge–discharge testing represents a commonly employed and accurate method for determining capacitance. In most applications, when an external load is typically applied to a supercapacitor, the operational behavior of galvanostatic charge–discharge is more closely associated with its electrochemical behavior [66]. **Figure 6b** presents the typical galvanostatic charge–discharge curves of the fabricated supercapacitors, collected within a current density range of 50-500 mA/g. The galvanostatic charge–discharge curves of the NFRC-Ba separator exhibit superior symmetry, indicating its pre-eminent electrochemical performance. Simultaneously, the discharge curve of the NFRC-Ba separator demonstrates a larger IR drop, signifying its favorable equivalent series resistance.

Figure 6c depicts the electrochemical impedance spectroscopy (EIS) of the fabricated supercapacitors and their equivalent circuits. EIS results show that using the NFRC - Ba separator allows for rapid ion diffusion and charge - transfer processes. The internal resistance (Rs ≈ 3Ω) and charge - transfer resistance (Rct ≈ 12Ω) of the NFRC - Ba separator are considerably lower than those of the NKK30AC - 100 (Rs ≈ 6Ω, Rct ≈ 31Ω). Compared to the NKK30AC - 100, the NFRC - Ba separator has a lower Rs. Generally, Rs includes the intrinsic electronic resistance of the electrode material, the ohmic resistance of the electrolyte, and the interfacial resistance between the electrode and the current collector. Since the electrodes and electrolytes in each device are the same, the different Rs values of the fabricated supercapacitors can be attributed to the electrolyte's ohmic resistance. Due to the NFRC - Ba separator's smaller thickness and higher conductivity, it shows a lower electrolyte ohmic resistance. The Rct results suggest that the resistance for ions to transfer through the NFRC - Ba separator is relatively small. These findings confirm that the NFRC - Ba separator can effectively shorten ion - transport pathways through its mesoporous channels and internal cavities, thus facilitating the electrochemical kinetic processes of supercapacitors.

Calculated from typical galvanostatic charge - discharge curves, Figure 6d presents the specific capacitances of the single electrode for the NFRC - Ba separator and the NKK30AC - 100 separator at different current densities. As the current density increases from 50 mA/g to 500 mA/g, the specific capacitances of the NFRC - Ba separator reach 89.52 F/g, 87.36 F/g, 85.15 F/g, 82.25 F/g, 80.57 F/g, and 78.82 F/g respectively, which are higher than those of the NKK30AC - 100 separator at the same current densities, namely 85.28 F/g, 81.36 F/g, 79.42 F/g, 77.36 F/g, 75.83 F/g, and 73.62 F/g. Clearly, the capacitance of the NFRC - Ba separator is significantly higher than that of the NKK30AC - 100 separator. This can be mainly attributed to its better electrolyte wettability and larger space for electrolyte ion transport. When the current density increases to 500 mA/g, the capacitance retention rate of the SC - NFRC - Ba is about 87.48%, which is notably higher than that of the NKK30AC - 100 separator.

Moreover, cycle durability is one of the most crucial features of a high - performance separator[67]. **Figure 6e** shows the results of long - term cycling tests conducted at a current density of 1 A/g in a 1.0 M sodium sulfate electrolyte. Even after 10000 cycles, the capacitance of the NFRC - Ba separator remains almost unchanged, demonstrating its excellent cycle durability. As shown in the inset of Figure 6f, the long - term cycling test of the NFRC - Ba separator reveals a relatively large IR drop. Additionally, the discharge curve of the SC - NKK30AC - 100 separator shows a larger IR drop compared to that of the NFRC - Ba separator, indicating that the IR drop is mainly caused by the electrode material. Moreover, after 10000 cycles, the NFRC - Ba separator still maintains its original morphology. The outstanding cycle stability of the NFRC - Ba separator indicates its stability and durability when used as a supercapacitor separator. However, due to the large IR drop, the previously assembled supercapacitors cannot undergo galvanostatic charge - discharge tests at high current densities.

 doi:10.20944/preprints202502.1660.v1

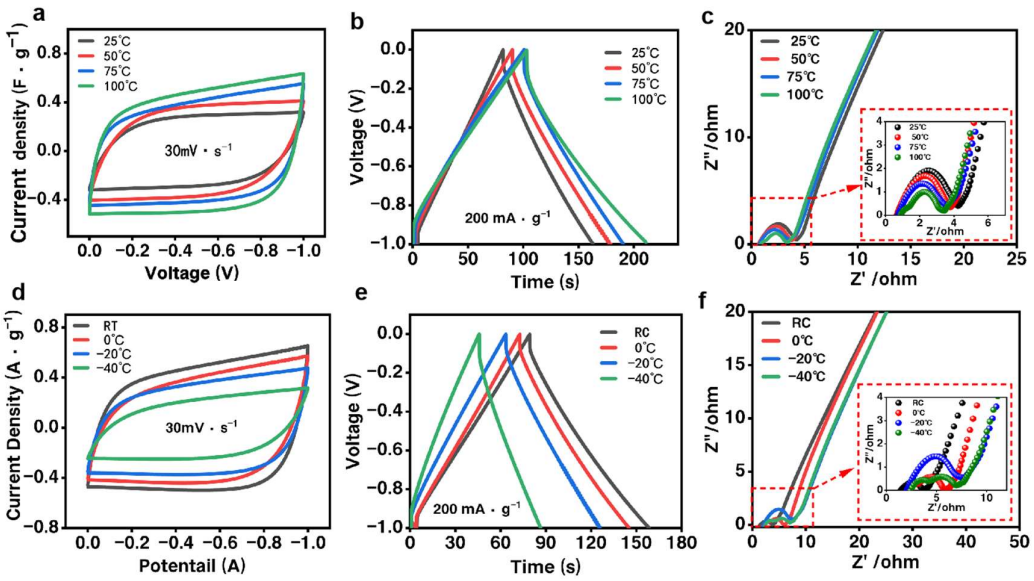

Figure 7. Comparison of Electrochemical Properties between the NFRC - Ba Separator and the Commercial NKK30AC - 100 Separator at 25 - 100 °C: (a) Cyclic voltammograms (CVs) of NFRC - Ba at a scan rate of 30 mV/ s; (b) Galvanostatic charge - discharge (GCD) curves of NFRC - Ba at a current density of 500 mA /g; (c) Electrochemical impedance spectroscopy (EIS) curves of NFRC - Ba. Comparison of Electrochemical Properties between the NFRC - Ba Separator and the Commercial NKK30AC - 100 Separator at RC - (-40) °C: (d) Cyclic voltammograms (CVs) of NFRC - Ba at a scan rate of 30 mV/ s; (e) Galvanostatic charge - discharge (GCD) curves of NFRC - Ba at a current density of 500 mA/g; (f) Electrochemical impedance spectroscopy (EIS) curves of NFRC - Ba.

The application suitability of the fabricated supercapacitors with the NFRC-Ba separator was tested under different environmental conditions, ranging from high to low temperatures. The capacitance behavior of the device was investigated within a temperature ranges of 25-100 °C and from room temperature to -40 °C. **Figure 7a** shows the cyclic voltammetry (CV) curves of the fabricated supercapacitors in the temperature interval from 25 °C to 100 °C. Calculated from the typical CV curves, at a scan rate of 30 mV/s, the specific capacitances of the SC-NFRC-Ba were 63.29 F/g, 75.84 F/g, 79.23 F/g, and 82.38 F/g, respectively. As the test temperature increased, the capacitance of the NFRC-Ba separator increased due to the enhanced charge mobility in the electrolyte. Moreover, its CV curve retained a rectangular shape, indicating that, due to the outstanding thermal stability of this separator, no internal current leakage or side reactions occurred.

The adaptability of the fabricated supercapacitors equipped with the NFRC-Ba separator across a wide gamut of temperature conditions, ranging from high to low, was meticulously explored. Specifically, their electrochemical behaviors were probed within two temperature intervals, 25 °C～100 °C, and from room temperature (RC) to -40 °C. As illustrated in **Figure 7a**, an increase in temperature leads to an expansion of the area enclosed by the cyclic voltammetry (CV) curve, while its original rectangular shape is maintained. This suggests that the NFRC-Ba separator showcases favorable ionic conductivity under elevated temperatures. The high-temperature galvanostatic charge–discharge curves, measured at a current density of 30 mA/g (as shown in Figure 7b), exhibit a quasi-triangular profile similar to that at room temperature. Notably, the charge–discharge time increases at higher temperatures. The specific capacitances measured at 25 °C, 50 °C, 75 °C, and 100 °C are 63.29 F/g, 75.84 F/g, 79.23 F/g, and 82.38 F/g, respectively, evidencing remarkable capacitance performance. Figure 7c depicts the electrochemical impedance spectroscopy (EIS) curves of the NFRC-Ba separator within the 25 °C～100 °C temperature range. In the low-frequency domain, the curves remain nearly vertical across almost all temperatures within this range, highlighting the stable charge-transfer ability of the NFRC-Ba separator. This stability can be attributed to the separator's

 doi:10.20944/preprints202502.1660.v1

exceptional adaptability to high-temperature conditions. Owing to the accelerated ion transport at high temperatures, the diffusion resistance of the supercapacitor decreases as the temperature rises. The reduction in interfacial contact resistance with increasing temperature is somewhat restricted, decreasing from 6 Ω at 25 °C to 3 Ω at 100 °C. Conversely, the decrease in series resistance is more substantial. As the temperature increases from 25 °C to 100 °C, the series resistance drops from 12 Ω to 8 Ω, mainly because of the enhanced ionic conductivity of the NFRC-Ba separator at high temperatures.

As presented in **Figure 7d**, as the temperature drops from RC to -40 ° C, the area encircled by the cyclic voltammetry (CV) curve decreases slightly. However, it still maintains its initial rectangular form, suggesting that the NFRC-Ba separator can still demonstrate favorable ionic conductivity under low-temperature conditions. The galvanostatic charge–discharge curves obtained at low temperatures, measured at a current density of 30 mA/g (**Figure 7e**), display a quasi-triangular shape comparable to that at RC. Moreover, the charge–discharge duration shortens as the temperature decreases. The specific capacitances measured at RC, 0 ° C, -20 ° C, and -40 ° C are 62.2 F/g, 53.4 F/g, 49.8 F/g, and 41.7 F/g, respectively. Compared to the capacitance at RC, the capacitance retention ratios at 0 ° C, -20 ° C, and -40 ° C are 86%, 80%, and 67%, respectively, indicating excellent capacitance performance. **Figure 7f** illustrates the electrochemical impedance spectroscopy curves of the NFRC-Ba separator within a temperature range from RC to -40 ° C. Notably, in the low-frequency zone, the curves remain almost vertical across nearly all temperatures in this range, reflecting the stable charge-transfer capacity of the NFRC-Ba separator. This stability can be attributed to the separator's outstanding adaptability to low-temperature environments. Due to the slower ion transportation at low temperatures, the diffusion resistance of the supercapacitor increases as the temperature falls. The growth of the interfacial contact resistance with the decrease in temperature is limited, increasing from 3 Ω at RC to 7 Ω at -40 ° C. In contrast, the increase in series resistance is more substantial. When the temperature decreases from RC to -40 ° C, the series resistance climbs from 6 Ω to 18 Ω, mainly because of the reduced ionic conductivity of the NFRC-Ba separator at low temperatures.

4. Discussion

The article starts by highlighting the pivotal role of supercapacitor separators in the fast-growing electronics and new-energy fields. It points out the flaws of traditional separators, initiating the search for new ones. Beginning with cellulose-based materials, it details the preparation of a NFRC-Ba composite regenerated cellulose separator. Then, it comprehensively assesses its performance via multiple tests, covering physical properties (mechanical strength, porosity, hydrophilicity, thermal stability), ionic properties (ionic conductivity, ion-transport ability), and charge–discharge performance (specific capacitance, capacitance retention, cycle durability, performance at various temperatures). Contrasting it with commercial separators showcases the NFRC-Ba separator's advantages. Overall, given its performance and preparation process, the NFRC-Ba separator shows great potential as a commercial material for high-performance, high-safety supercapacitors and other capacitors.

Author Contributions: Conceptualization, C.Z. and H.L.; methodology, H.L.; software, H.L. and F.Z; validation, H.L.; formal analysis, H.L.; investigation, H.L.; resources, H.L.; data curation, H.L.; writing—original draft preparation, H.L.; writing—review and editing, H.L. and J.L.; visualization, H.L.; supervision, C.Z. and F.Z.; project administration, C.Z. and F.Z.; funding acquisition, C.Z. All authors have read and agreed to the published version of the manuscript.

Funding: This research received no external funding.

Institutional Review Board Statement: Not applicable.

Data Availability Statement: Not applicable.

Acknowledgments: The data presented in this study are available on request from the authors.

Conflicts of Interest: The authors declare no conflicts of interest.

 doi:10.20944/preprints202502.1660.v1

References

1. Kwade, A., W. Haselrieder. Current status and challenges for automotive battery production technologies. *Nat Energy*, **2018**. *3*(4)290-300.https://10.1038/s41560-018-0130-3
2. Cano, Z. P., D. Banham. Batteries and fuel cells for emerging electric vehicle markets. *Nat Energy*, **2018**. *3*(4)279-289.https://10.1038/s41560-018-0108-1
3. Simon, P. and Y. Gogotsi. Materials for electrochemical capacitors. *Nat. Mater*, **2008**. *7*(11)845-854.https://10.1038/nmat2297
4. Sharma, S. and P. Chand. Supercapacitor and electrochemical techniques: A brief review. *Results in Chemistry*, **2023**. *5*100885.https://doi.org/10.1016/j.rechem.2023.100885
5. Saher, S., S. Johnston. Trimodal thermal energy storage material for renewable energy applications. *Nature*, **2024**. *636*(8043)622-626.https://10.1038/s41586-024-08214-1
6. Du, X., Z. Lin. Electrode Materials, Structural Design, and Storage Mechanisms in Hybrid Supercapacitors. *Molecules*, **2023**. *28*(17)6432
7. Hong, X., J. He. Recent advance in electrochemically activated supercapacitors: Activation mechanisms, electrode materials and prospects. *Renewable Sustainable Energy Rev.*, **2025**. *209*115134. https://doi.org/10.1016/j.rser.2024.115134
8. Carrascosa, A., J. S. Sánchez. Advanced Flexible Wearable Electronics from Hybrid Nanocomposites Based on Cellulose Nanofibers, PEDOT:PSS and Reduced Graphene Oxide. *Polymers*, **2024**. *16*(21)3035
9. Huang, X., R. He. Functionalized separator for next-generation batteries. *Materials Today*, **2020**. *41*143-155.https://doi.org/10.1016/j.mattod.2020.07.015
10. Lagadec, M. F., R. Zahn, and V. Wood. Characterization and performance evaluation of lithium-ion battery separators. *Nat Energy*, **2019**. *4*(1)16-25.https://10.1038/s41560-018-0295-9
11. Xing, J., S. Bliznakov. A Review of Nonaqueous Electrolytes, Binders, and Separators for Lithium-Ion Batteries. *Electrochem. Energy Rev.*, **2022**. *5*(4)14.https://10.1007/s41918-022-00131-z
12. Hu, W., W. Fu. Heat-resistant Al2O3 nanowire-polyetherimide separator for safer and faster lithium-ion batteries.
13. *J MATER SCI TECHNOL*, **2023**. *142*112-120.https://doi.org/10.1016/j.jmst.2022.09.015
14. Zhong, S., B. Yuan. Recent progress in thin separators for upgraded lithium ion batteries. *Energy Storage Materials*, **2021**. *41*805-841.https://doi.org/10.1016/j.ensm.2021.07.028
15. Liu, J.-H., P. Wang. Review on electrospinning anode and separators for lithium ion batteries. *RENEW SUST ENERG REV*, **2024**. *189*113939.https://doi.org/10.1016/j.rser.2023.113939
16. Chai, Y., D. Ning. Construction of flexible asymmetric composite polymer electrolytes for high-voltage lithium metal batteries with superior performance. *Nano Energy*, **2024**. *130*110160.https://doi.org/10.1016/j.nanoen.2024.110160
17. Tang, L., B. Chen. Polyfluorinated crosslinker-based solid polymer electrolytes for long-cycling 4.5 V lithium metal batteries. *Nat. Commun.*, **2023**. *14*(1)2301.https://10.1038/s41467-023-37997-6
18. Huang, J., C. Xu. Non-Flammable fluorinated gel polymer electrolyte for safe lithium metal batteries in harsh environments. *J. Colloid Interface Sci.*, **2025**. *683*984-993.https://doi.org/10.1016/j.jcis.2024.12.103
19. Zhang, Z., H. Hu. The Application of Porous Carbon Derived from Furfural Residue as the Electrode Material in Supercapacitors. *Polymers*, **2024**. *16*(23)3421
20. Li, H., D. Wu. Flexible, High-Wettability and Fire-Resistant Separators Based on Hydroxyapatite Nanowires for Advanced Lithium-Ion Batteries. *Adv. Mater.*, **2017**. *29*(44)1703548.https://doi.org/10.1002/adma.201703548
21. Chen, X., F. Chu. In Situ Polymerized Fluorine-Free Ether Gel Polymer Electrolyte with Stable Interface for High-Voltage Lithium Metal Batteries. *Adv. Funct. Mater.***2024.**2421965.https://doi.org/10.1002/adfm.202421965
22. Cheng, X. and J. Bae. Recent Advancements in Fabrication, Separation, and Purification of Hierarchically Porous Polymer Membranes and Their Applications in Next-Generation Electrochemical Energy Storage Devices. *Polymers*, **2024**. *16*(23)3269
23. Zhang, T.-W., J.-L. Chen. Sustainable Separators for High-Performance Lithium Ion Batteries Enabled by Chemical Modifications. *Adv. Funct. Mater.*, **2019**. *29*(28)1902023.https://doi.org/10.1002/adfm.201902023

24. Yang, Y. and J. Zhang. Highly Stable Lithium–Sulfur Batteries Based on Laponite Nanosheet-Coated Celgard Separators. *Adv. Energy Mater.*, **2018**. *8*(25)1801778.https://doi.org/10.1002/aenm.201801778
25. Huang, Z., Y. Chen. Vapor-induced phase inversion of poly (m-phenylene isophthalamide) modified polyethylene separator for high-performance lithium-ion batteries. *Chem. Eng. J.* **2022**. *429*132429. https://doi.org/10.1016/j.cej.2021.132429
26. Schadeck, U., K. Kyrgyzbaev. Flexible, Heat-Resistant, and Flame-Retardant Glass Fiber Nonwoven/Glass Platelet Composite Separator for Lithium-Ion Batteries. *Energies*, **2018**. *11*(4)999
27. Hsia, T.-N., H.-C. Lu. Superdry poly(vinylidene fluoride-co-hexafluoropropylene) coating on a lithium anode as a protective layer and separator for a high-performance lithium-oxygen battery. *J. Colloid Interface Sci.*, **2022**. *626*524-534.https://doi.org/10.1016/j.jcis.2022.06.172
28. Cao, J., D. Zhang. Manipulating Crystallographic Orientation of Zinc Deposition for Dendrite-free Zinc Ion Batteries. *Adv. Energy Mater.*, **2021**. *11*(29)2101299.https://doi.org/10.1002/aenm.202101299
29. Dong, T., W. U. Arifeen. Surface-modified electrospun polyacrylonitrile nano-membrane for a lithium-ion battery separator based on phase separation mechanism. *Chem. Eng. J.* **2020**. *398*125646.https://doi.org/10.1016/j.cej.2020.125646
30. Zhou, C., Q. He. A robust electrospun separator modified with in situ grown metal-organic frameworks for lithium-sulfur batteries. *Chem. Eng. J.* **2020**. *395*124979.https://doi.org/10.1016/j.cej.2020.124979
31. Raza, N., K. Aziz. Advancements in separator design for supercapacitor technology: A review of characteristics, manufacturing processes, limitations, and emerging trends. *J. Energy Storage*, **2025**. *111*115328. https://doi.org/10.1016/j.est.2025.115328
32. Yu, H., Q. Tang. Using eggshell membrane as a separator in supercapacitor.J. Power Sources, **2012**. *206*463-468. https://doi.org/10.1016/j.jpowsour.2012.01.116
33. Kalluri, L., J. A. Griggs. Preparation and optimization of an eggshell membrane-based biomaterial for GTR applications. *Dent. Mater.*, **2024**. *40*(4)728-738. https://doi.org/10.1016/j.dental.2024.02.008
34. Zhang, Y., J. He. Converting eggs to flexible, all-solid supercapacitors. *Nano Energy*, **2019**. *65*104045. https://doi.org/10.1016/j.nanoen.2019.104045
35. Bai, S., B. Kim. Permselective metal–organic framework gel membrane enables long-life cycling of rechargeable organic batteries. *Nat. Nanotechnol.*, **2021**. *16*(1)77-84. https://10.1038/s41565-020-00788-x
36. Wenshuai, C., Y. Haipeng. Nanocellulose: a promising nanomaterial for advanced electrochemical energy storage. *Chem. Soc. Rev.*, **2018**. *47*(8)2837-2872. https://doi.org/10.1039/C7CS00790F
37. Doobary, S., V. A. Kalkavoura. Nanocellulose: New horizons in organic chemistry and beyond. *Chem*, **2024**. *10*(11)3279-3293. https://10.1016/j.chempr.2024.09.007
38. El-Shafai, N. M., M. M. Ibrahim. Synthesis, characterization, and cytotoxicity of self-assembly of hybrid nanocomposite modified membrane of carboxymethyl cellulose/graphene oxide for photocatalytic antifouling, energy storage, and supercapacitors application. *COLLOID SURFACE A*, **2021**. *626*127035.https://doi.org/10.1016/j.colsurfa.2021.127035
39. Moreira, R., R. C. Rebelo. Novel thermally regenerated flexible cellulose-based films. *Eur. J. Wood Wood Prod.*, **2024**. *82*(6)1813-1826. https://10.1007/s00107-024-02126-7
40. Chen, L., H. Yin. Stretchable, self-healing, adhesive and anti-freezing ionic conductive cellulose-based hydrogels for flexible supercapacitors and sensors. *Cellulose*, **2024**. *31*(18)11015-11033. https://10.1007/s10570-024-06226-8
41. Huan Song 1 , J. Y., Yu Yang 2 , Qing Yang 2 , Jian Hu Characterization of cellulose-nanofiber-modified fibrillated lyocell fiber separator. *BioResources*, **2022**. *17*(3)4689-4704. https://10.15376/biores.17.3.4689-4704
42. Shen, Y., G. Yang. Effect of lyocell fiber cross-sectional shape on structure and properties of lyocell/PLA composites. *J. Polym. Eng.*, **2022**. *42*(9)868-875. https://doi:10.1515/polyeng-2022-0070
43. Xiwen, W., H. Jian, and L. Jin. Preparation Ultra-fine Fibrillated Lyocell Fiber and Its Application in Battery Separator. *Int. J. Electrochem. Sci.*, **2011**. *6*(10)4999-5004.https://doi.org/10.1016/S1452-3981(23)18383-0
44. Wang, Y., J. Luo. Effect of fibrillated fiber morphology on properties of paper-based separators for lithium-ion battery applications.J. Power Sources, **2021**. *482*228899.https://doi.org/10.1016/j.jpowsour.2020.228899

45. Ding, Z., X. Yang, and Y. Tang. Nanocellulose-based electrodes and separator toward sustainable and flexible all-solid-state supercapacitor.Int. J. Biol. Macromol., **2023**. *228*467-477.https://doi.org/10.1016/j.ijbiomac.2022.12.224
46. Yu, R., P. M.N. High-throughput extraction of cellulose nanofibers from Imperata cylindrica grass for advanced bio composites.Int. J. Biol. Macromol., **2025**. *284*138111.https://doi.org/10.1016/j.ijbiomac.2024.138111
47. Antunes, B. D. F., L. R. Santana. Cellulose, cellulose nanofibers, and cellulose acetate from Butia fruits (Butia odorata): Chemical, morphological, structural, and thermal properties.Int. J. Biol. Macromol., **2024**. *281*136151. https://doi.org/10.1016/j.ijbiomac.2024.136151
48. Wu, Q., C. Jiang. Cellulose nanofiber-based hybrid hydrogel electrode with superhydrophilicity enabling flexible high energy density supercapacitor and multifunctional sensors.Int. J. Biol. Macromol., **2024**. *276*134003. https://doi.org/10.1016/j.ijbiomac.2024.134003
49. Yuan, T., Z. Zhang. Cellulose nanofiber/MXene (Ti3C2Tx)/liquid metal film as a highly performance and flexible electrode material for supercapacitors.Int. J. Biol. Macromol., **2024**. *262*130119.https://doi.org/10.1016/j.ijbiomac.2024.130119
50. Yang, Z., Y. Wang. A morphology control engineered strategy of Ti3C2Tx/sulfated cellulose nanofibril composite film towards high-performance flexible supercapacitor electrode.Int. J. Biol. Macromol., **2023**. *243*124828. https://doi.org/10.1016/j.ijbiomac.2023.124828
51. Chen, Y., Y. Duan. Preparation of Bio-Based Foams with a Uniform Pore Structure by Nanocellulose/Nisin/Waterborne-Polyurethane-Stabilized Pickering Emulsion. *Polymers*, **2022**. *14*(23)5159
52. Li, H., H. Wang. Thermal-Responsive and Fire-Resistant Materials for High-Safety Lithium-Ion Batteries. *Small*, **2021**. *17*(43)2103679. https://doi.org/10.1002/smll.202103679
53. Zhou, D., L. Zhang. Novel Method to Achieve Temperature-Stable Microwave Dielectric Ceramics: A Case in the Fergusonite-Structured NdNbO4 System. *ACS Appl. Mater. Interfaces*, **2023**. *15*(15)19129
54. Jin, S., Z. Chen. Highly reversible Zn anode enabled by porous BaSO4 coating with wide band gap and high dielectric constant.J. Power Sources, **2024**. *591*233894.https://doi.org/10.1016/j.jpowsour.2023.233894
55. Zhang, Y., L. Cheng. Reversible Li plating regulation on graphite anode through a barium sulfate nanofibers-based dielectric separator for fast charging and high-safety lithium-ion battery. *J. Energy Chem.*, **2025**. *101*511-523. https://doi.org/10.1016/j.jechem.2024.08.053
56. Gonzalez, M. S., Q. Yan. Draining Over Blocking: Nano-Composite Janus Separators for Mitigating Internal Shorting of Lithium Batteries. *Adv. Mater.*, **2020**. *32*(12)1906836. https://doi.org/10.1002/adma.201906836
57. Zhang, J., Z. Liu. Renewable and Superior Thermal-Resistant Cellulose-Based Composite Nonwoven as Lithium-Ion Battery Separator. *ACS Appl. Mater. Interfaces*, **2013**. *5*(1)128-134. https://10.1021/am302290n
58. Song, T. and Y. Min. Electrospun polyimide nanofiber-based separators containing carboxyl groups for lithium-ion batteries.*J. Appl. Polym. Sci.*, **2024**. *141*(31)e55721.https://doi.org/10.1002/app.55721
59. Yuan, B., K. Wen. Composite Separators for Robust High Rate Lithium Ion Batteries. *Adv. Funct. Mater.*, **2021**. *31*(32)2101420.https://doi.org/10.1002/adfm.202101420
60. Wang, J., Y. Liu. Hierarchically Porous Silica Membrane as Separator for High-Performance Lithium-Ion Batteries. *Adv. Mater.*, **2022**. *34*(3)2107957.https://doi.org/10.1002/adma.202107957
61. Du, H., X. Zhou. Regulating Built-in Polar States via Atomic Self-Hybridization for Fast Ion Diffusion Kinetics in Potassium Ion Batteries. *Chin. J. Chem.*, **2024**. *42*(21)2589-2598.https://doi.org/10.1002/cjoc.202400335
62. Wang, X., S. Li. Hubbard Gap Closure-Induced Dual-Redox Li-Storage Mechanism as the Origin of Anomalously High Capacity and Fast Ion Diffusivity in MOFs-Like Polyoxometalates. *ANGEW CHEM INT EDIT*, **2025**. *64*(4)e202416735. https://doi.org/10.1002/anie.202416735
63. Liu, M., K. Turcheniuk. Scalable, safe, high-rate supercapacitor separators based on the Al2O3 nanowire Polyvinyl butyral nonwoven membranes. *Nano Energy*, **2020**. *71*104627. https://doi.org/10.1016/j.nanoen.2020.104627
64. Zahn, R., M. F. Lagadec. Improving Ionic Conductivity and Lithium-Ion Transference Number in Lithium-Ion Battery Separators. *ACS Appl. Mater. Interfaces*, **2016**. *8*(48)32637-32642.https://10.1021/acsami.6b12085

 doi:10.20944/preprints202502.1660.v1

65. Jiang, S., Z. Lan. Mechanisms by Which Exogenous Substances Enhance Plant Salt Tolerance through the Modulation of Ion Membrane Transport and Reactive Oxygen Species Metabolism. *Antioxidants*, **2024**. *13*(9)1050
66. Lin, Y.-C., H.-H. Chen. Massively Enhanced Charge Selectivity, Ion Transport, and Osmotic Energy Conversion by Antiswelling Nanoconfined Hydrogels. *Nano Letters*, **2024**. *24*(37)11756-11762.https://10.1021/acs.nanolett.4c03836
67. Gojgić, J., M. Petrović. Electrochemical and Electrical Performances of High Energy Storage Polyaniline Electrode with Supercapattery Behavior. *Polymers*, **2022**. *14*(24)5365
68. Park, H. G., J. J. Jeong. Ion-Conducting Robust Cross-Linked Organic/Inorganic Polymer Composite as Effective Binder for Electrode of Electrochemical Capacitor. *Polymers*, **2022**. *14*(23)5174